ARMY RESEARCH LABORATORY

Molecular Modeling of Energetic Materials: The Parameterization and Validation of Nitrate Esters in the COMPASS Force Field

by Steven W. Bunte and Huai Sun

ARL-TR-2364 November 2000

The findings in this report are not to be construed as an official Department of the Army position unless so designated by other authorized documents.

Citation of manufacturer's or trade names does not constitute an official endorsement or approval of the use thereof.

Destroy this report when it is no longer needed. Do not return it to the originator.

Army Research Laboratory
Aberdeen Proving Ground, MD 21005-5066

ARL-TR-2364 **November 2000**

Molecular Modeling of Energetic Materials: The Parameterization and Validation of Nitrate Esters in the COMPASS Force Field

Steven W. Bunte
Weapons and Materials Research Directorate, ARL

Huai Sun
Molecular Simulations, Inc.

Abstract

To investigate the mechanical and other condensed phase properties of energetic materials using atomistic simulation techniques, the COMPASS force field has been expanded to include high-energy nitro functional groups. This report presents the parameterization and validation of COMPASS for nitrate esters ($-ONO_2$). The functional forms of this force field are of the consistent force field type. The parameters were derived with an emphasis on the nonbonded parameters, which include a Lennard-Jones 9-6 function for the van der Waals (vdW) term and a Coulombic term for an electrostatic interaction. To validate the force field, molecular mechanics calculations and molecular dynamics simulations have been made on a variety of molecules containing the nitrate ester functionality. Using this force field, excellent agreement has been obtained between the calculated and experimental values for molecular structures, vibrational frequencies, liquid densities, heats of vaporization, crystal structure, mechanical properties and lattice energy.

Acknowledgments

This work was supported in part by a grant of computer time at the DOD Major Shared Resource Center located at the U.S. Army Research Laboratory. The authors also acknowledge the assistance of Dr. Maggie Hurley and Tomeka Spence of the ARL Programming Environment and Training Program in performing some of the conformational energy computations.

INTENTIONALLY LEFT BLANK.

Table of Contents

INTENTIONALLY LEFT BLANK.

List of Figures

INTENTIONALLY LEFT BLANK.

List of Tables

INTENTIONALLY LEFT BLANK

1. Introduction

The ballistic performance of a propellant in a gun system is known to be dependent upon the mechanical response of the propellant grains to the high stress and high strain environment experienced during the interior ballistic cycle. In addition, although not totally understood, the vulnerability of a propellant, which is the response of the propellant to a variety of stimulii such as impact and heat, is known to be influenced by the mechanical properties of the material. Generally speaking, poor mechanical properties yield poor vulnerability results; however, good mechanical properties don't always yield good vulnerability results. In numerical models of the interior ballistic process, the propellant grain is considered to be an incompressible, nondeformable solid that burns with a mass generation rate that is determined by the measured burn rate and the exposed surface area. If grain fracture occurs, more surface area is exposed, which results in an increase in the expected mass generation rate. This can lead to decreased performance, or in the worst case scenario, complete failure. Our objective in initiating this study is to develop the capability to use molecular modeling techniques to characterize the physical properties of high-energy materials at the atomistic level. The information gained from this modeling effort can help direct changes in the formulation and the processing techniques used in the manufacturing of the propellant, which may ultimately result in improving the performance and vulnerability properties of the propellant.

For modeling the properties of large molecular systems and condensed phases, molecular modeling techniques that are force field based have distinct advantages over *ab initio* methodologies. This is not only because the force field method is several orders of magnitude faster than any *ab initio* method, but also because the information that an *ab initio* method provides is often not necessary for these applications. The properties of interest are generally the result of the statistical average of atomistic movement over a much longer time scale than the rapid electron motion that an *ab initio* method describes. In addition, the most important interaction terms in simulating the condensed phase are the nonbonding forces (in particular, the dispersion forces), which are extremely difficult to accurately describe using *ab initio* methods. Reports have recently appeared which document the accurate prediction of a wide variety of properties of molecules in both the condensed phase and in isolation using the COMPASS

(condensed-phase optimized molecular potentials for atomistic simulation studies) force field [1–2]. Popular force fields, such as MM3 [3–13], AMBER [14–15], and CHARMM [16], have been designed mainly to study biologically interesting molecules. The COMPASS force field, on the other hand, has been specifically designed for material science applications. It is a class II *ab initio* force field in that it employs complex functional forms and is derived from extensive *ab initio* data. Consequently, it can be used to accurately predict several molecular properties, including molecular structures, conformations, and vibrations. The nonbonded parameters in COMPASS have been optimized using condensed-phase (liquid and crystal) data so that several thermophysical properties of molecular liquids and crystals can be well reproduced. It is important to note that COMPASS has been developed to model the static properties of condensed phase molecules. It is not designed to study reactions; the development of a reactive force field is a significant undertaking and is outside the scope of this work. COMPASS has broad coverage in the major application areas of material science. It has been parameterized to study most common organic molecules, organic and inorganic polymers, zeolites, and metal/transition-metal oxides. However, some of the functional groups required to model energetic materials have not until now been parameterized and included in the COMPASS force field. For instance, a common propellant is composed of three principal energetic ingredients: nitrocellulose (NC, $C_6H_{7.55}N_{2.45}O_{9.90}$), nitroglycerin (NG, O_2NOCH_2-$CHONO_2$-$CH2ONO_2$), and diethyleneglycol dinitrate (DEGDN, O_2NO-$(CH_2)_2$-O-$(CH_2)_2$-ONO_2). In the propellant blend, the NC is present as an energetic binder and NG serves as an energetic gelling agent. DEGDN is also an energetic ingredient; however, it also plays the role of a plasticizing agent in the propellant. The common chemical feature in each of these compounds is the nitrate ester (-ONO_2) functional group. Compounds containing nitro (-NO_2) are currently parameterized in the COMPASS force field and contain most, but not all, of the parameters needed to model the nitrate esters. This work reports on the parameterization and validation of the additional atom types needed to model the nitrate ester functional group in the COMPASS force field.

2. Force Field Development

***2.1 Ab Initio* Calculations.** Very few high quality measurements of the molecular structures and conformations have been reported for high energy compounds containing the nitrate ester

functional group. Since experimental data is lacking, the validation of the force field has to be based on accurate *ab initio* data. In order to determine the level of calculation that is reasonable both in terms of accuracy and computational expense, we carried out an evaluation of several candidate *ab initio* methods. This was done by performing a series of calculations on two model nitrate ester compounds, methyl and ethyl nitrate, as shown in Figure 1, and included both the trans and gauche conformers of ethyl nitrate. The following levels of theory were used: HF/6-31g(d), HF/6-311g(d,p), MP2/6-311g(d, p), MP2/6-311g(2df, 2p), SVWN/6-311g(d, p), and B3LYP/6-311g(d, p). These calculations were carried out using the GAUSSIAN 94 (G94) [17] suite of quantum chemistry programs running on a Silicon Graphics Origin 2000 located at the U.S. Army Research Laboratory Major Shared Resource Center. The calculations were completed using the default convergence criteria for all methods and the default grid sizes for the DFT methods contained in G94. Table 1 lists the calculated results at the different levels of theory and the experimental data for methyl nitrate, while Tables 2 and 3 list the calculated results and experimental data for the trans and gauche conformers of ethyl nitrate, respectively. The calculated energies of the ethyl nitrate conformers are presented in Tables 2 and 3. In addition, the energy difference between the trans and gauche conformer at each level of theory is presented in Table 3.

A comparison of the calculated structure of methyl nitrate at the various levels of theory with the experimental structure determined by Cox and Waring [18] yields the following results: the HF/6-31g(d) and HF/6-311g(d,p) bond lengths are within 2% of experiment, and the bond angles are within 0.9% of experiment; the MP2/6-311g(d,p) and the MP2/6-311g(2df,2p) bond lengths are within 0.4% of experiment, and the bond angles are within 0.4% of experiment; the SVWN/6-311g(d,p) bond lengths are within 1.2% of experiment, and the bond angles are within 0.8%; and finally, the B3LYP/6-311g(d,p) bond lengths and bond angles are both within 0.5% of experiment. Similar agreement is observed between our calculations and the results obtained from the microwave studies of Scroggin et al. [19] on ethyl nitrate. An analysis of the calculated energies of ethyl nitrate shows the difference between the isomers to be 0.73 kcal/mole at HF/6-31g(d), 0.76 kcal/mole at HF/6-311g(d,p), 0.18 kcal/mole at MP2/6-311g(d,p), 0.22 kcal/mole at B3LYP/6-311g(d,p), and 0.13 kcal/mole at MP2/6-311g(2df,2p). In each of these calculations, the trans conformer is predicted to be more stable than the gauche conformer.

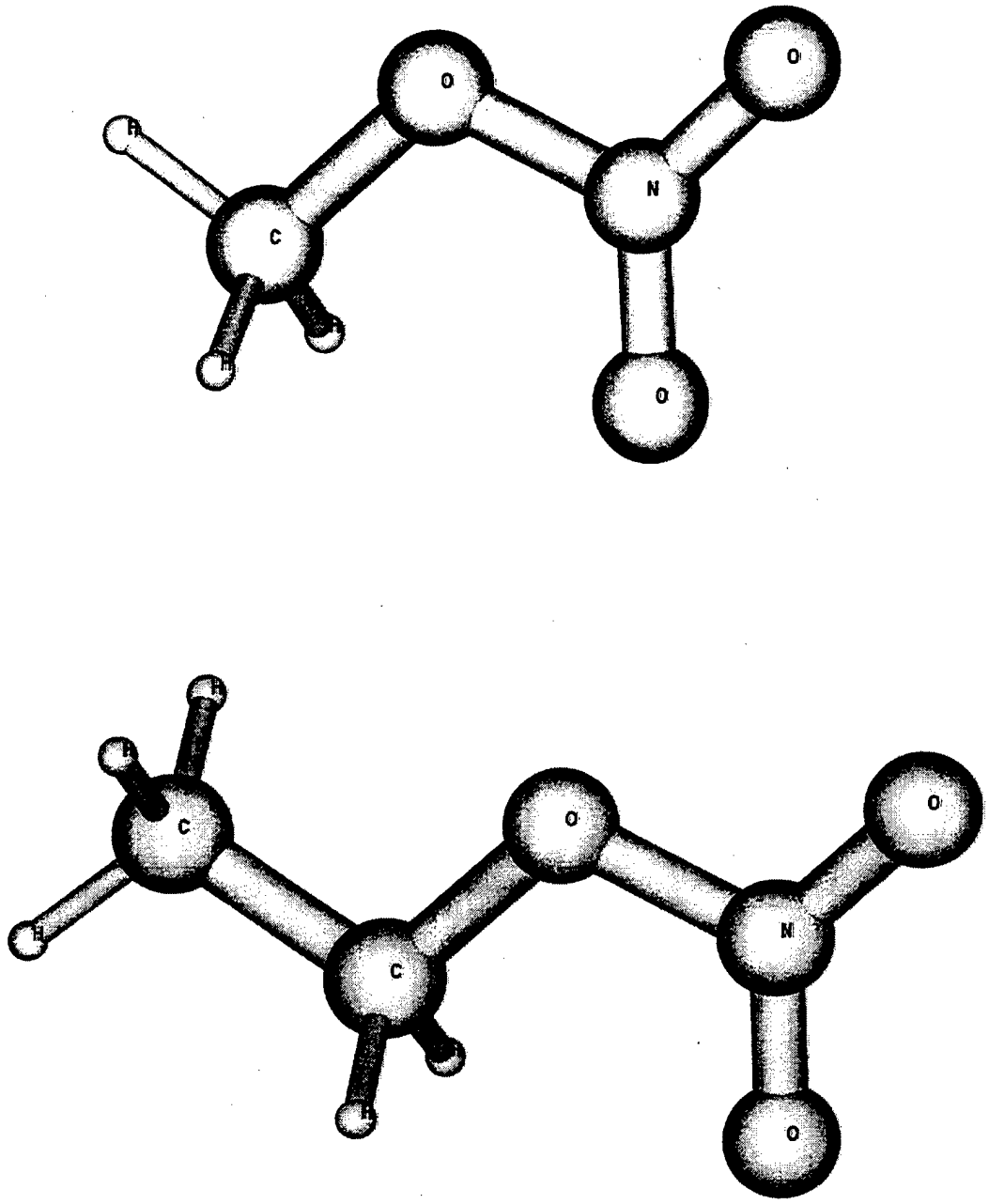

Figure 1. Methyl and Ethyl Nitrate.

Table 1. Optimized Geometries of Methyl Nitrate

	Exp[a]	HF/6-31g(d)	HF/6-311g(d,p)	MP2/6-311g(d,p)	MP2/6-311g(2df,2p)	SVWN/6-311g(d,p)	B3LYP/6-311g(d,p)	Force Field
Internal Coordinates (Å)								
C1-O2	1.437	1.428	1.427	1.431	1.427	1.410	1.438	1.437
O2-N3	1.402	1.330	1.330	1.414	1.406	1.425	1.424	1.416
N3-O4	1.208	1.177	1.169	1.211	1.209	1.202	1.207	1.210
N3-O5	1.205	1.187	1.180	1.205	1.202	1.192	1.197	1.208
C1-H6	1.088	1.078	1.079	1.091	1.086	1.101	1.090	1.100
C1-H7	1.095	1.078	1.079	1.091	1.086	1.101	1.09	1.100
C1-H8	—	1.077	1.078	1.089	1.084	1.098	1.089	1.100
Simple Angles (°)								
C1-O2-N3	112.7	115.8	116.0	112.6	112.1	112.0	113.5	114.2
O2-N3-O4	118.1	114.0	113.9	112.4	112.5	112.6	112.6	113.0
O2-N3-O5	118.1	117.9	117.8	117.3	117.1	116.3	117.2	117.1
H6-C1-O2	103.4	103.2	103.3	103.1	103.6	103.9	103.2	109.3
H7-C1-O2	110.4	110.5	110.5	111.2	111.2	111.5	111.1	110.2
H8-C1-O2	—	110.5	110.6	111.2	111.2	111.5	111.1	110.2
Dihedral Angles (°)								
C1-O2-N3-O4	—	179.9	-180.0	-180.0	-180.0	-180.0	-180.0	-180.0
C1-O2-N3-O5	—	0.0	0.0	0.0	0.0	0.0	0.0	0.0

[a]Experiment from reference [18].

Table 2. Optimized Geometries of the Trans Conformer of Ethyl Nitrate

	Exp[a]	HF/6-31g(d)	HF/6-311g(d,p)	MP2/6-311g(d,p)	MP2/6-311g(2df,2p)	SVWN/6-311g(d,p)	B3LYP/6-311g(d,p)	Force Field
Internal Coordinates (Å)								
C1-C2	1.521	1.513	1.512	1.516	1.509	1.496	1.517	1.527
C2-O3	1.439	1.439	1.438	1.438	1.435	1.424	1.450	1.439
O3-N4	1.402	1.328	1.328	1.414	1.404	1.417	1.419	1.409
N4-O5	1.201	1.178	1.170	1.205	1.203	1.194	1.198	1.206
N4-O6	1.210	1.187	1.181	1.212	1.209	1.204	1.208	1.209
C2-H7	1.089	1.079	1.080	1.093	1.088	1.104	1.092	1.103
C2-H8	1.089	1.079	1.080	1.093	1.088	1.104	1.092	1.103
C1-H9	1.094	1.083	1.084	1.092	1.086	1.100	1.091	1.101
C1-H10	1.093	1.084	1.085	1.093	1.087	1.100	1.093	1.102
C1-H11	1.093	1.083	1.084	1.092	1.086	1.100	1.091	1.102
Simple Angles (°)								
C1-C2-O3	103.6	105.4	105.6	105.1	105.1	105.7	105.6	106.8
C2-O3-N4	115.8	116.4	116.6	113.2	112.9	112.8	114.2	112.2
O3-N4-O5	114.0	114.0	114.0	112.4	112.6	112.7	112.7	113.3
O3-N4-O6	116.9	118.0	118.0	117.4	117.3	116.6	117.4	116.8
H7-C2-C1	112.3	112.3	112.2	111.8	112.0	112.4	112.1	110.6
H8-C2-C1	112.3	112.3	112.2	111.8	112.0	112.4	112.1	110.6
H9-C1-C2	109.2	110.9	110.9	110.6	110.7	111.0	111.0	110.9
H10-C1-C2	110.9	109.1	109.0	109.2	109.4	109.8	109.2	110.9
H11-C1-C2	110.9	110.9	110.9	110.6	110.7	111.0	111.0	110.8
Dihedral Angles (°)								
C1-C2-O3-N4	180.0	−180.0	−180.0	−180.0	−180.0	180.0	−180.0	−180.0
C2-O3-N4-O5	—	180.0	180.0	180.0	180.0	−180.0	−180.0	180.0
C2-O3-N4-O6	—	0.0	0.0	0.0	0.0	0.0	0.1	0.0
Calculated Energy (Hartrees)								
	—	−357.514120	−357.610177	−358.693092	−358.889389	−357.818687	−359.612682	−0.038791

[a]Experiment from reference [20].

Table 3. Optimized Geometries of the Gauche Conformer of Ethyl Nitrate

	Exp[a]	HF/6-31g(d)	HF/6-311g(d,p)	MP2/6-311g(d,p)	MP2/6-311g(2df,2p)	SVWN/6-311g(d,p)	B3LYP/6-311g(d,p)	Force Field
Internal Coordinates (Å)								
C1-C2	1.523	1.515	1.514	1.518	1.510	1.499	1.519	1.529
C2-O3	1.442	1.441	1.440	1.440	1.437	1.424	1.452	1.440
O3-N4	1.403	1.330	1.329	1.414	1.404	1.424	1.422	1.411
N4-O5	1.200	1.177	1.169	1.205	1.203	1.192	1.197	1.206
N4-O6	1.211	1.187	1.181	1.212	1.210	1.204	1.208	1.209
C2-H7	1.088	1.079	1.079	1.092	1.087	1.101	1.091	1.103
C2-H8	1.088	1.077	1.078	1.092	1.086	1.103	1.090	1.103
C1-H9	1.095	1.082	1.082	1.091	1.086	1.100	1.091	1.102
C1-H10	1.091	1.085	1.086	1.094	1.088	1.101	1.094	1.101
C1-H11	1.094	1.084	1.084	1.092	1.087	1.100	1.092	1.101
Simple Angles (°)								
C1-C2-O3	107.2	111.9	112.1	112.2	112.0	112.2	112.4	108.7
C2-O3-N4	117.4	117.2	117.5	113.8	113.3	113.0	114.9	113.5
O3-N4-O5	112.2	113.8	113.9	112.2	112.4	112.5	112.5	113.1
O3-N4-O6	119.7	118.4	118.3	117.8	117.7	117.0	117.8	117.1
H7-C2-C1	110.7	111.5	111.5	111.5	111.5	112.2	111.8	112.3
H8-C2-C1	113.5	112.7	112.5	112.1	112.1	111.8	112.2	109.5
H9-C1-C2	109.1	111.4	111.4	111.1	111.0	110.7	111.2	110.2
H10-C1-C2	110.9	109.1	108.9	109.6	109.6	110.2	109.5	110.6
H11-C1-C2	111.1	110.5	110.5	110.0	110.3	110.6	110.6	112.1
Dihedral Angles (°)								
C1-C2-O3-N4	81.7	-80.2	-79.9	-78.0	-78.7	-77.9	-80.9	-78.6
C2-O3-N4-O5	—	177.8	177.8	176.3	176.7	176.9	177.5	177.2
C2-O3-N4-O6	—	-2.5	-2.5	-4.2	-3.8	-3.5	-3.0	-3.1
Calculated Energy (Hartrees)								
	—	-357.512954	-357.6089597	-358.6927981	-358.8891785	-357.819648	-359.612335	-0.037944
Trans-Gauche Energy Difference (kcal/mol)								
	—	0.73	0.76	0.18	0.13	-0.60	0.22	0.53

[a]Experiment from reference [20].

These results are consistent with the calculations reported by Durig and Sheehan [20]. The exception in our series of calculations is at the SVWN/6-311g(d,p) level of theory where the gauche isomer is calculated to be the more stable of the two by 0.6 kcal/mole. The B3LYP/6-311g(d,p) method yields good results for the molecular structures of the model nitrates and for the conformational energy differences of ethyl nitrate, with considerably lower computational requirements than the MP2 calculations. This method provides an ideal combination of accuracy and efficiency; consequently, the B3LYP/6-311g(d,p) method was used throughout the remainder of this study for validating the structures of additional nitrate esters, such as NC, NG, and DEGDN, for which little experimental data is available.

2.2 Parameterization Method. The functional forms of the COMPASS 1.0 force field are the same as the CFF-type force fields [21–29], as in

$$
\begin{aligned}
E_{\text{total}} &= \sum_{b}\left[k_2(b-b_o)^2 + k_3(b-b_o)^3 + k_4(b-b_o)^4\right] \\
&+ \sum_{\theta}\left[k_2(\theta-\theta_o)^2 + k_3(\theta-\theta_o)^3 + k_4(\theta-\theta_o)^4\right] \\
&+ \sum_{\phi}\left[k_1(1-\cos\phi) + k_2(1-\cos 2\phi) + k_3(1-\cos 3\phi)\right] \\
&+ \sum_{\chi} k_2(\chi-\chi_o)^2 \\
&+ \sum_{b,b'} k(b-b_o)(b'-b'_o) \\
&+ \sum_{b,\theta} k(b-b_o)(\theta-\theta_o) \\
&+ \sum_{b,\phi} (b-b_o)\left[k_1\cos\phi + k_2\cos 2\phi + k_3\cos 3\phi\right] \\
&+ \sum_{\theta,\phi} (\theta-\theta_o)\left[k_1\cos\phi + k_2\cos 2\phi + k_3\cos 3\phi\right] \\
&+ \sum_{b,\theta} k(\theta'-\theta'_o)(\theta-\theta_o) \\
&+ \sum_{\theta,\theta,\phi} k(\theta-\theta_o)(\theta'-\theta'_o)(\phi-\phi_o) \\
&+ \sum_{i,j}\frac{q_i q_j}{r_{ij}} \\
&+ \sum_{i,j}\varepsilon_{ij}\left[2\left(\frac{r_{ij}^o}{r_{ij}}\right)^9 - 3\left(\frac{r_{ij}^o}{r_{ij}}\right)^6\right].
\end{aligned}
\tag{1}
$$

The potential functions can be divided into two categories—valence terms including the diagonal and off-diagonal cross coupling terms and the nonbonded interaction terms. The valence terms include E_b, E_θ, E_ϕ, and E_χ for bond, angle, torsion, and out-of-plane angle coordinates, respectively, and $E_{bb'}$, $E_{b\theta}$, $E_{b\phi}$, $E_{\theta\theta'}$, and $E_{\theta\theta\phi}$ represent the cross-coupling terms between internal coordinates. The cross-coupling terms are important for predicting vibrational frequencies and structural variations associated with conformational changes. Among the cross-coupling terms, the bond–bond $E_{bb'}$, bond–angle $E_{b\theta}$, and bond–torsion $E_{b\phi}$ are the most significant. The nonbonded terms, which include a "soft" Lennard-Jones 9–6 (L-J) potential for the van der Waals (vdW) interaction and a Coulombic term for the electrostatic interactions, are used for interactions between pairs of atoms that are separated by three or more intervening atoms, or those that belong to different molecules. The L-J parameters (ϵ and r°) for like atom pairs are adjustable parameters. For unlike atom pairs, a sixth order combination law [30] is used to calculate the off-diagonal parameters as follows:

$$r_{i,j}^\circ = \left[\frac{\left(r_i^\circ\right)^6 + \left(r_j^\circ\right)^6}{2}\right]^{\frac{1}{6}}, \tag{2}$$

and

$$\varepsilon_{i,j} = 2\sqrt{\varepsilon_i \cdot \varepsilon_j}\left[\frac{\left(r_i^\circ\right)^3 \cdot \left(r_j^\circ\right)^3}{\left(r_i^\circ\right)^6 + \left(r_j^\circ\right)^6}\right]. \tag{3}$$

The electrostatic interaction is represented by the partial atomic charge model using charge bond-increments, δ_{ij}, as a measure of the charge separation between two valence-bonded atoms. The net partial charge of an atom, q_i, is obtained as a summation of all charge-bond increments related to this atom:

$$q_i = \sum_j \delta_{ij} \tag{4}$$

The details on the methodology of parameterization are reported elsewhere [1, 2]. Basically, the valence parameters (both diagonal and off-diagonal cross-coupling terms) and charge-bond increments were derived by least-squares fitting to the HF/6-31g(d) data calculated for the model compounds methyl and ethyl nitrate. The *ab initio* data includes electrostatic potentials, energies, and the first and second derivatives of the energies. The resulting parameters were subsequently scaled by a set of generic factors to correct the systematic errors of the HF/6-31g(d) calculations. The resulting force field (quantum mechanics force field or QMFF) was then systematically validated and modified to fit experimental or higher-level *ab initio* data for molecules in isolation. The vdW nonbonded parameters (L-J 9–6 terms) were initially transferred from other organic systems [21, 22, 25–28, 31, 32]. After the valence parameters were derived, they were subject to optimization using MD simulations of liquids. The whole validation and optimization procedure was repeated until a consistent fit was obtained for both the gaseous and condensed phases.

2.3 Molecular Dynamics Simulations. Molecular dynamics (MD) simulations were carried out using the software package InsightII/Discovery. For liquids and crystals, a periodic cell with explicit minimum image convention [33, 34] was built for each of the model compounds studied. The cubic cell edges ranged in length from 20 to 30 Å and contained 1000 to 1500 atoms. A charge-group-based cutoff method with tail correction was used to evaluate the nonbonded interactions in all of the liquid simulations. It is assumed in the charge-group-based cutoff method that the radial distribution functions converged to unity beyond the cutoff distance [33, 34], which in our simulations was 9.5 Å. For the crystal simulations, the Ewald summation method [33, 34] was used for both the vdW and the electrostatic terms. Constant volume and temperature (NVT) ensembles, with a velocity Verlet integrator [33, 34] and Andersen's [35, 36] temperature control method, were used for the parameterization. Constant pressure and temperature (NPT) simulations were carried out using a modified velocity Verlet [33, 34] integrator with the Berendsen [37] pressure control method for the validation calculations. A time step of 1 fs was used in all of the MD simulations.

The initial configuration of the liquid being simulated was constructed using the following procedure. First, molecules were uniformly placed into a cubic cell that was large enough so that

there was no strong repulsion between any two molecules. The system was then randomized by running a NVT simulation for several hundred steps at a temperature of 2000 K, which is well over the boiling point of all of the liquids studied. Following randomization, the system was gradually compressed to the target density in a high pressure (5,000–50,000 bar) NPT simulation. Finally, a pre-equilibrium process was performed using a simulated annealing technique, during which the temperature was gradually reduced from 2000 K to 300 K. The pre-equilibration took about 50–100 ps, which is usually adequate for liquids of small molecules [1, 2]. The average periods were 50 ps for NVT simulations and 100 ps for NPT simulations.

3. Parameterization

3.1 Valence Parameters. As stated previously, the valence parameters were derived from *ab initio* data using a least squares fitting procedure [1, 2]. Simple nitro-containing (-NO_2) compounds (such as nitrobenzene and nitro-alkanes), which share most of the same parameters with the nitrate esters, were parameterized in the COMPASS 1.0 force field [1, 2]. In this project, additional model compounds, methyl and ethyl nitrate, were calculated at the HF/6-31g(d) level of theory to sample the "missing" interaction energy terms. To maintain consistency with the other COMPASS parameters, the HF/6-31g(d) data were used to derive the missing valence parameters, which due to historic limitation, were derived at the same level of theory since the early 1990's. The systematic errors between the HF/6-31g(d) calculations and experimental measurements have been well documented [21–29], and a set of scaling factors that correct the errors have been established and implemented throughout the development of COMPASS. With the additional data, the remaining valence parameters were derived with an accuracy level similar to the other systems that have been parameterized and reported previously [1, 2]. The new parameters were then subjected to the same empirical adjustment procedure to yield a better overall fit of the structural and conformational properties of the molecules in isolation. The final parameters for nitro-containing compounds are given in the Appendix. Three atom types [1, 2] are used for these compounds: n3o for the nitrogen atom of the nitro group, o12 for the oxygen atoms in the nitro group, and o2n for the ester oxygen in the nitrate ester. Note that only n3o is a specific atom type for the nitro moiety; both o12 and o2n are equivalent to the more generic atom types, o2 and o1, for the valence terms [1, 2]. Together with

the atom types and parameters defined for alkanes and benzenes [1, 2], the parameters provide complete coverage of simple nitro-containing compounds and nitrate esters.

3.2 Atomic Partial Charges. As a significant part of the parameterization of the nonbonded terms, atomic partial charges have drawn considerable attention during the development of the COMPASS force field. Generally speaking, a constrained fitting of the electrostatic potential [1, 2] (CESP) is used to derive the atomic partial charges. This approach ensures the transferability of the charge parameters, while maintaining an overall best fit of the *ab initio* electrostatic potential energy surfaces. The actual partial charges for nitrous acid, methyl nitrite, nitrobenzene, methyl nitrate, and ethyl nitrate, obtained from both Mulliken analysis and CESP fitting, are listed in Table 4 for comparison. The CESP charges are represented by bond charge increments (δ_{ij}) which represent the charge flow between two adjacent atoms, i and j, as given in the Appendix. Several parameters (for alkanes and benzenes) are transferred and fixed during the CESP fitting procedure; a single bond-charge increment applies to all compounds containing the same chemical bond (eg., one $\delta_{n3o,o1=}$ for all N-O bonds in the nitro group and the nitrate group). Consequently, the partial charges obtained are more "symmetric" than those obtained from the Mulliken analysis. Despite the enforced constraints in the CESP fit, the overall quality of the reproduced *ab initio* electrostatic potential energy surfaces is satisfactory. This can be measured by calculating the root mean square (RMS) errors (in kcal/mol) between the *ab initio* electrostatic potentials and the potentials calculated using the partial charges. The RMS errors are presented in Table 5. Using the CESP charges, the calculated RMS errors in the ESP are significantly smaller than those calculated using the Mulliken charges. An additional evaluation of the electrostatic parameters is given in Table 6, where the molecular dipole moments calculated using the Mulliken and CESP charges are compared against experimental and *ab initio* results. Although the dipole moments were not used as input data for fitting, the CESP charges reproduce these values reasonably well.

3.3 The van der Waals (vdW) Parameters. With the valence and charge parameters fully determined, the only remaining terms to be addressed are the weak vdW interactions. These terms, which are known to play a critical role in the simulation of condensed phases, were

Table 4. Comparison of Atomic Partial Charges

Nitrous Acid (HNO_2)		
	Mullikan	CESP
N1	0.427	0.668
O2	-0.412	-0.428
O3	-0.412	-0.428
H11	0.396	0.188

Methyl Nitrite (CH_3NO_2)		
	Mullikan	CESP
N1	0.561	0.646
O2	-0.453	-0.428
O3	-0.456	-0.428
C1	-0.350	0.051
H11	0.233	0.053
H12	0.232	0.053
H13	0.232	0.053

Nitrobenzene ($C_6H_5NO_2$)		
	Mullikan	CESP
N1	0.520	0.617
O2	-0.469	-0.428
O3	-0.475	-0.428
C4	0.171	0.239
C5	-0.173	-0.127
H6	0.274	0.127
C7	-0.216	-0.127
H8	0.222	0.127
C9	-0.171	-0.127
H10	0.222	0.127
C11	-0.219	-0.127
H12	0.222	0.127
C13	-0.181	-0.127
H14	0.273	0.127

Methyl Nitrate (CH_3ONO_2)		
	Mullikan	CESP
N1	0.959	0.857
O2	-0.475	-0.428
O3	-0.438	-0.428
O4	-0.475	-0.317
C1	-0.197	0.158
H11	0.212	0.053
H12	0.206	0.053
H13	0.206	0.053
—	—	—
—	—	—
—	—	—
—	—	—
—	—	—
—	—	—

Ethyl Nitrate ($C_2H_5ONO_2$)		
	Mullikan	CESP
O2	-0.501	-0.317
N1	0.973	0.857
O3	-0.443	-0.428
O3	-0.476	-0.428
C1	-0.018	0.211
C1	-0.511	-0.159
H11	0.203	0.053
H11	0.203	0.053
H11	0.183	0.053
H12	0.193	0.053
H13	0.193	0.053
—	—	—
—	—	—
—	—	—

Table 5. RMS Errors (kcal/mol) Between *Ab Initio* ESPs and ESPs From Partial Charges

Molecule	Mulliken	CESP
HNO_2	2.397	0.735
CH_3NO_2	3.491	0.771
$C_6H_5NO_2$	3.666	1.367
CH_3ONO_2	2.502	0.860
$C_2H_5ONO_2$	2.840	0.951

Table 6. Comparison of Calculated and Experimental Molecular Dipole Moments

Molecule	HF/6-31g(d)	Mulliken	CESP	Experiment
HNO_2	3.028	3.978	3.038	—
CH_3NO_2	4.048	5.958	3.994	—
$C_6H_5NO_2$	5.031	7.635	4.574	—
CH_3ONO_2	3.835	5.060	3.896	3.081[a]
$C_2H_5ONO_2$	4.125	5.374	3.931	3.39[b] (trans) 3.23[b] (gauche)

[a]Reference [18].
[b]Reference [19].

subject to parameterization using condensed phase data. The Lennard-Jones 9–6 (L-J) function is used for representing the van der Waals energies. Most of the nonbonded vdW parameters are transferred from alkanes, ethers, and nitro compounds [1, 2]. In this project, only one new atom type (o2n) was introduced, which requires two new vdW parameters (the L-J well depth, ϵ, and the vdW radii, r^o) to be defined. We selected liquid methyl, ethyl, propyl, isopropyl, and butyl nitrate to be used in the determination of these parameters. The thermophysical properties of density, ρ, and the heat of vaporization, ΔH_v, of these liquids were calculated. The heat of vaporization was obtained from the cohesive energy density (E_{CED}) by use of the following equation:

$$\Delta H_V = E_{CED} \cdot M / \rho + RT, \quad (5)$$

where M is the molecular weight and ρ is the density. The parameterization process consisted of repeated MD simulations during which the adjustable parameters (ε and r^o) were modified. By comparing the calculated pressures and the cohesive energies at a given temperature against the experimental data, the optimized parameters were identified numerically from 5 to 10 data points.

4. Validation

4.1 Gas Phase Molecular Properties. The validation of molecular properties for molecules in the gas phase was based on the molecular mechanics calculations. These calculations were performed on the isolated (i.e., gas phase) molecules of methyl and ethyl nitrate. In each case, the calculations consisted of full-energy minimizations followed by calculation of the Hessian matrix. These results were compared with either the experimental data or with the results from high-level *ab initio* calculations.

4.1.1 Structures. The most basic property to predict is the structure of the molecule. It is well known, for example, that a small deviation in the bond length can have a potentially significant effect on the liquid or crystal density obtained from an MD simulation. Consequently, prior to running the condensed phase simulations, it is extremely important to make sure that the structural properties are accurately modeled using the force field. As shown in Tables 1, 2, and 3, the present force field yields excellent agreement with experiment and high-level *ab initio* calculations on methyl and ethyl nitrate. The average deviation of the experimental bond lengths, obtained using the force field, is 0.5% for methyl nitrate and 0.6% for each of the conformers of ethyl nitrate. The bond angles differ on average by 1.4% for methyl nitrate, 1.5% for the gauche conformer of ethyl nitrate, and 1.3% for the trans conformer. For the larger molecules (NG and DEGDN), similar results were obtained. A graph of the force-field-calculated bond lengths and bond angles of DEGDN and NG are plotted vs. the B3LYP/6-311g(d,p) results in Figures 2 and 3, respectively. There are a total of 39 data points for the bond

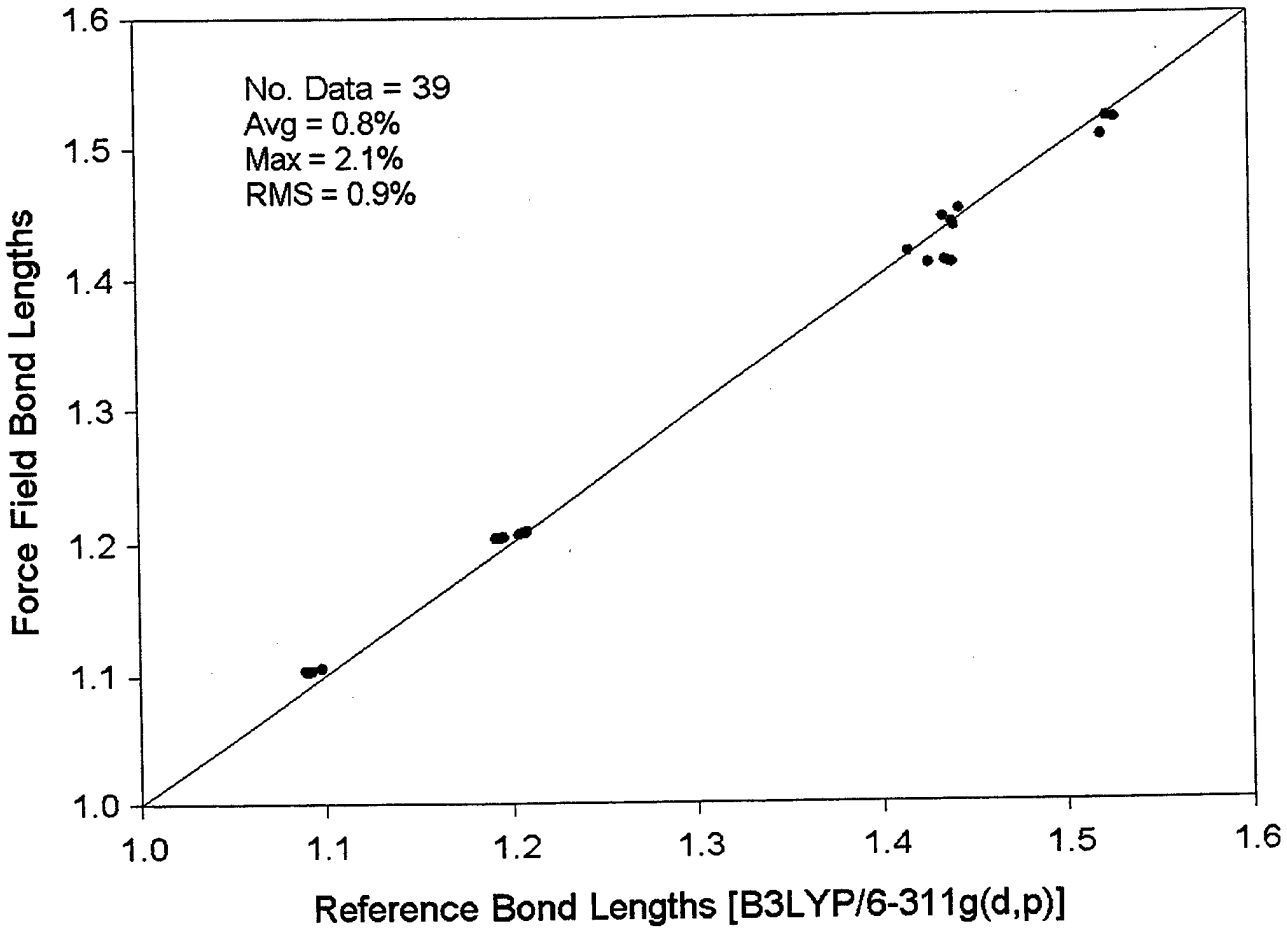

Figure 2. Comparison of the Bond Lengths (in Å) of NG and DEGDN Calculated Using the Force Field and the B3LYP/6-311g(d,p) Reference.

lengths and 21 for the bond angles. As indicated in the figures, excellent agreement between the calculated (force field) and reference (B3LYP) data is obtained. The average percentage deviation in the bond lengths is 0.8%, and the maximum percentage deviation is 2.1%. The root mean squares (RMS) percentage deviation is 0.9%. For the bond angles, the average percentage deviation is 1.1%, with a maximum percentage deviation of 3.0%. The RMS percentage deviation is 1.3%. These results are consistent with the results obtained on other molecules using the COMPASS force field [1, 2].

4.1.2 Vibrational Frequencies. A molecular mechanics (MM) force field is different from a spectroscopic force field. Generally speaking, by simultaneously fitting various properties

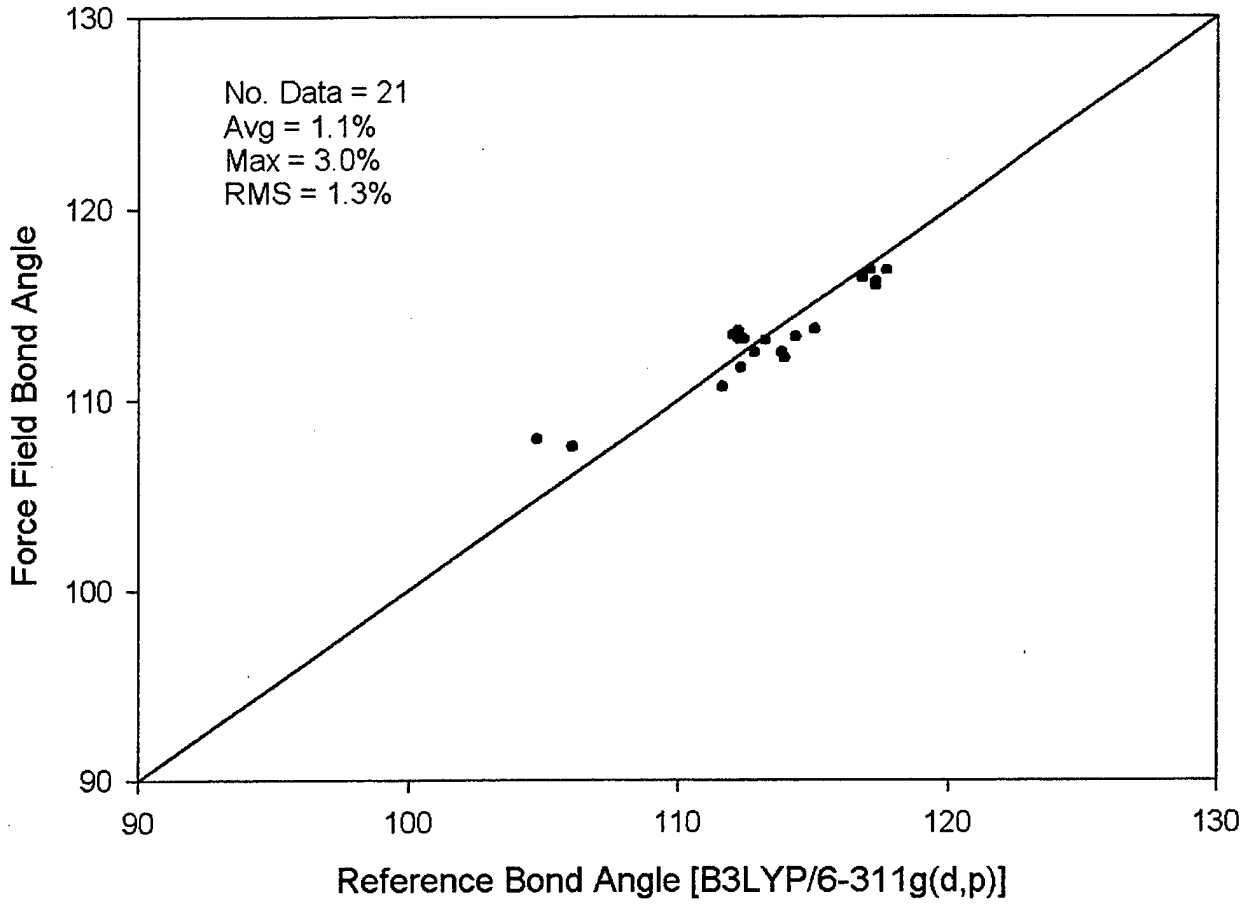

Figure 3. Comparison of the Bond Angles (in Degrees) of NG and DEGDN Calculated Using the Force Field and the B3LYP/6-311g(d,p) Reference.

including structures, conformations, and vibrational frequencies, a MM force field can only predict the vibrational frequencies with a modest level of accuracy (a RMS deviation of approximately 20–50 cm^{-1}). Frequency predictions obtained by COMPASS generally fall into this category. In Tables 7–9, the vibrational frequencies of methyl and ethyl nitrate, calculated using the force field, are compared with experimentally determined frequencies [20, 38] and with frequencies computed at the B3LYP/6-311g(d,p) and MP2/6-311g(d,p) levels of theory. In addition, approximate descriptions of the modes are also presented. As shown, the COMPASS-calculated frequencies agree reasonably well with the experimental values. The methyl nitrate frequencies have an average deviation of –3.4 cm^{-1} from the experimental values, with a maximum deviation of 94 cm^{-1}. The RMS deviation in the methyl nitrate frequencies is

Table 7. Calculated and Experimental Vibrational Frequencies (cm^{-1}) of Methyl Nitrate

Mode	Experimental[a]	MP2/6-311g(d,p)	B3LYP/6-311g(d,p)	COMPASS	Approx. Description[a]
1	3034	3223	3153	2988	CH_3 stretch
2	3015	3196	3130	2987	CH_3 stretch
3	2966	3099	3049	2902	CH_3 stretch
4	1668	1877	1741	1727	NO_2 stretch
5	1469	1532	1501	1469	CH_3 deformation
6	1457	1497	1472	1453	CH_3 deformation
7	1435	1491	1463	1435	CH_3 deformation
8	1291	1323	1333	1385	NO_2 stretch
9	1178	1213	1190	1151	CH_3 rock
10	1156	1198	1167	1133	CH_3 rock
11	1019	1081	1020	1113	CO stretch
12	855	875	871	944	ON stretch
13	761	767	769	743	NO_2 rock
14	658	688	663	604	NO_2 deformation
15	571	592	572	484	NO_2 wag
16	344	357	340	310	CON bend
17	204	234	200	212	CH_3 torsion
18	134	138	141	113	NO_2 torsion

[a]Reference [38].

52.6 cm^{-1}. For the ethyl nitrate (including both the trans and gauche conformers) frequencies, the average deviation is –13.2 cm^{-1}, and the maximum deviation is 81 cm^{-1}. The RMS deviation is 40.1 cm^{-1}. The statistical analysis was computed for 18 methyl nitrate frequencies and 54 ethyl nitrate frequencies. For NG and DEGDN, the force field and B3LYP/6-311g(d,p) results were compared due to the lack of experimental data. In Figure 4, the COMPASS frequencies are plotted against the B3LYP frequencies. There are 111 data points plotted with an average deviation of –12.1 cm^{-1}. The maximum absolute deviation is –190.7 cm^{-1}, and the RMS deviation is 65.4 cm^{-1}. The largest deviations are found in the high frequency region (>3000 cm^{-1}), which correspond to the C-H stretch modes. By comparing the B3LYP/6-311g(d,p) frequencies against the experimental values for methyl and ethyl nitrates (as shown in Tables 7–9), it is clear that these deviations are largely due to the over estimates of C-H frequencies by the B3LYP/6-311g(d,p) method.

Table 8. Calculated and Experimental Vibrational Frequencies (cm^{-1}) of Ethyl Nitrate (Gauche Conformer)

Mode	Experimental[a]	MP2/6-311g(d,p)	B3LYP/6-311g(d,p)	COMPASS	Approx. Description[a]
1	2990	3203	3141	2971	CH_2 stretch
2	2986	3183	3134	2970	CH_3 stretch
3	2977	3178	3115	2964	CH_2 stretch
4	2949	3124	3108	2913	CH_3 stretch
5	2940	3090	3074	2901	CH_3 stretch
6	1660	1871	1734	1741	NO_2 stretch
7	1519	1529	1508	1522	CH_2 deformation
8	1460	1508	1488	1472	CH_3 deformation
9	1444	1505	1482	1461	CH_3 deformation
10	1392	1444	1419	1413	CH_3 deformation
11	1369	1414	1401	1397	CH_2 wag
12	1298	1347	1328	1368	CH_2 twist
13	1288	1317	1323	1283	NO_2 stretch
14	1270	1205	1183	1192	CH_2 rock
15	1161	1133	1109	1140	CH_3 rock
16	1092	1091	1029	1045	CC stretch
17	1025	939	910	969	CO stretch
18	903	868	860	873	CH_2 rock
19	809	819	807	775	NO stretch
20	765	765	767	744	NO_2 wag
21	643	765	649	612	NO_2 scissor
22	573	677	574	500	NO_2 rock
23	410	419	409	375	CCO bend
24	346	364	349	330	CON bend
25	199	229	225	221	CH_3 torsion
26	110	142	124	132	CO torsion
27	96	94	97	90	NO_2 torsion

[a]Reference [20].

4.1.3 Conformations. The equilibrium confirmations of methyl and ethyl nitrate are illustrated in Figure 1. The NO_2 group is coplanar with the C-O-N plane. The N-O bond has a partial double bond character, as indicated by the relatively high energy barrier of rotation for the NO_2 group around the N-O bond, as given in Figures 5 and 6. For both methyl and ethyl nitrate, the energy barrier heights are about 7 kcal/mol. This barrier is much lower than what is observed for a true double bond, but is significantly higher than that of a single bond. As seen in Figures 5

Table 9. Calculated and Experimental Vibrational Frequencies (cm^{-1}) of Ethyl Nitrate (Trans Conformer)

Mode	Experimental[a]	MP2/6-311g(d,p)	B3LYP/6-311g(d,p)	COMPASS	Approx. Description[a]
1	2990	3197	3126	2972	CH_2 stretch
2	2986	3185	3112	2969	CH_3 stretch
3	2977	3162	3098	2966	CH_2 stretch
4	2949	3104	3055	2912	CH_3 stretch
5	2940	3093	3044	2900	CH_3 stretch
6	1660	1873	1732	1741	NO_2 stretch
7	1519	1549	1525	1496	CH_2 deformation
8	1460	1522	1501	1468	CH_3 deformation
9	1444	1503	1484	1457	CH_3 deformation
10	1392	1448	1426	1410	CH_3 deformation
11	1369	1413	1403	1397	CH_2 wag
12	1298	1319	1324	1369	CH_2 twist
13	1288	1316	1294	1299	NO_2 stretch
14	1270	1205	1180	1197	CH_2 rock
15	1161	1170	1142	1125	CH_3 rock
16	1122	1085	1028	1063	CC stretch
17	1025	954	923	990	CO stretch
18	903	877	876	883	CH_2 rock
19	851	843	829	777	NO stretch
20	765	766	769	738	NO_2 wag
21	702	732	707	639	NO_2 scissor
22	566	583	569	494	NO_2 rock
23	378	386	373	333	CCO bend
24	242	263	254	255	CON bend
25	203	233	225	215	CH_3 torsion
26	120	125	130	118	NO_2 torsion
27	112	101	88	92	CO torsion

[a]Reference [20].

and 6, the COMPASS energy profile is in excellent agreement with the MP2/6-311g(d,p) and B3LYP/6-311g(d,p) results.

Figures 7 and 8 are the energy profiles for the rotations about the C-O bond in methyl and ethyl nitrate, respectively. The profile of methyl nitrate shows a low energy barrier height of

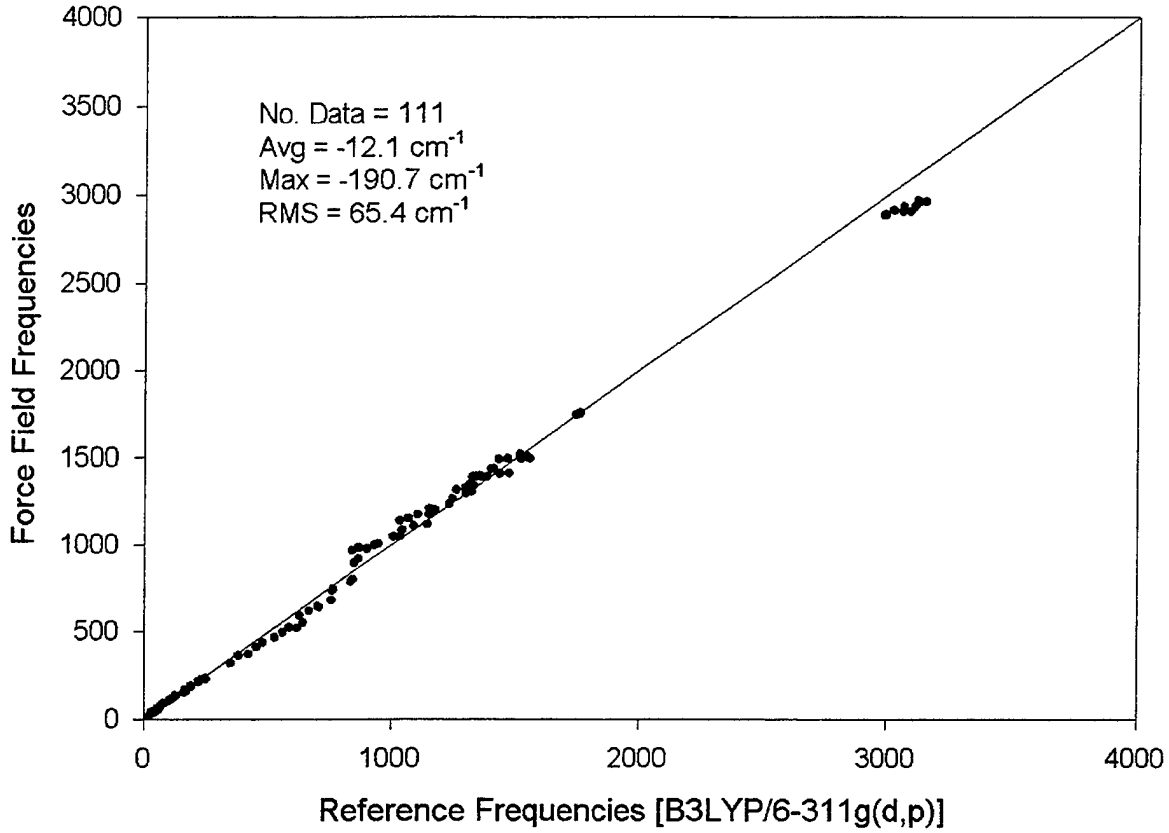

Figure 4. Comparison of the Vibrational Frequencies (in cm^{-1}) of NG and DEGDN Calculated Using the Force Field and the B3LYP/6-311 g(d,p) Reference.

about 2.5 kcal/mol, which is a typical value for a single bond. The rotation about the same C-O bond in ethyl nitrate, however, has a more complicated pattern. The global minimum structure has a C-C-O-N dihedral angle of 180°, which corresponds to the trans geometry. In addition, there is a local minimum located at a C-C-O-N dihedral angle of about 80° (gauche position). The trans to gauche isomerization energy barrier is approximately 2.0 kcal/mol; the transition state to this isomerization reaction has a C-C-O-N dihedral angle of roughly 120°. The guache to gauche isomerization has a barrier height of about 10 kcal/mol, and the transition state to this isomerization has a C-C-O-N dihedral angle of 0°. These results are in excellent agreement with the HF/6-31g(d) calculations of Durig and Sheehan [20]. Apparently, the high energy is largely due to nonbonded interactions (repulsion) between the methyl and NO_2 groups.

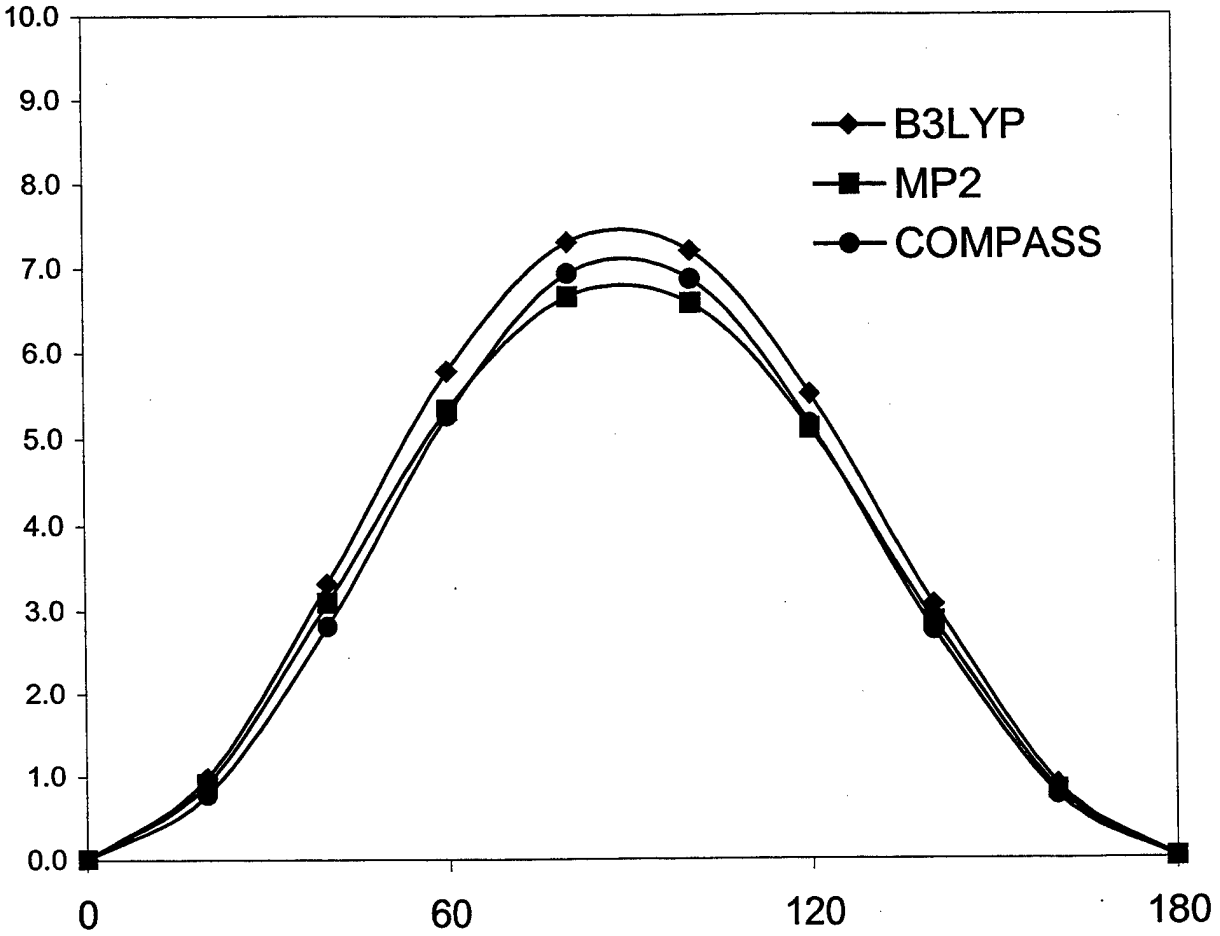

Figure 5. Energy (kcal/mol) Profile of the Rotation of the NO_2 Group About the O-N Bond of Methyl Nitrate.

4.2 Liquid Properties. With the final parameters, NPT simulations were performed to calculate the densities of the five selected liquid nitrate compounds at room temperature and at temperatures at or near their boiling point. The boiling point temperature for NG is not available in the literature; however, Stull [39] has measured the vapor pressure of NG over a range of temperatures from 400–524 K. This implies that NG is stable at these temperatures during the time frame in which the measurements were made. We arbitrarily chose a temperature of 450 K to run the elevated-temperature NG simulation, which is approximately in the middle of the range over which the experiment was conducted; the results are listed in Table 10. The experimental densities measured at room temperature are available for direct comparison. As

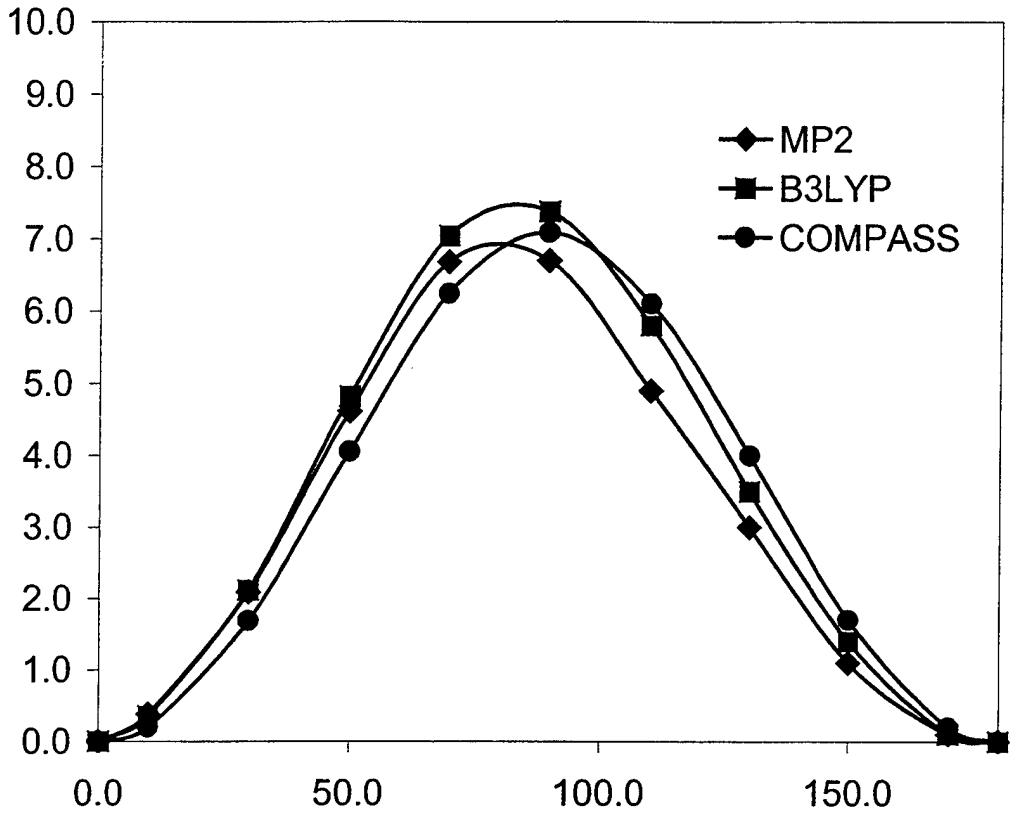

Figure 6. Energy (kcal/mol) Profile of the Rotation of the NO_2 Group About the O-N Bond of Ethyl Nitrate.

shown in the table, the agreements are excellent for most systems. The 3% deviation for isopropyl nitrate is slightly larger than normal. The reason is unclear at this point. We have not found any density information at the boiling point for direct comparison.

The values of the heats of vaporization were calculated using equation 5, with simulated densities at two temperatures for each of the molecular liquids. Most of the experimental data are derived from vapor pressures measured at room temperature. Our results calculated at room temperature and at elevated temperatures are in excellent agreement with the experimental data. The deviations are within the same normal range found in many molecules that COMPASS covers.

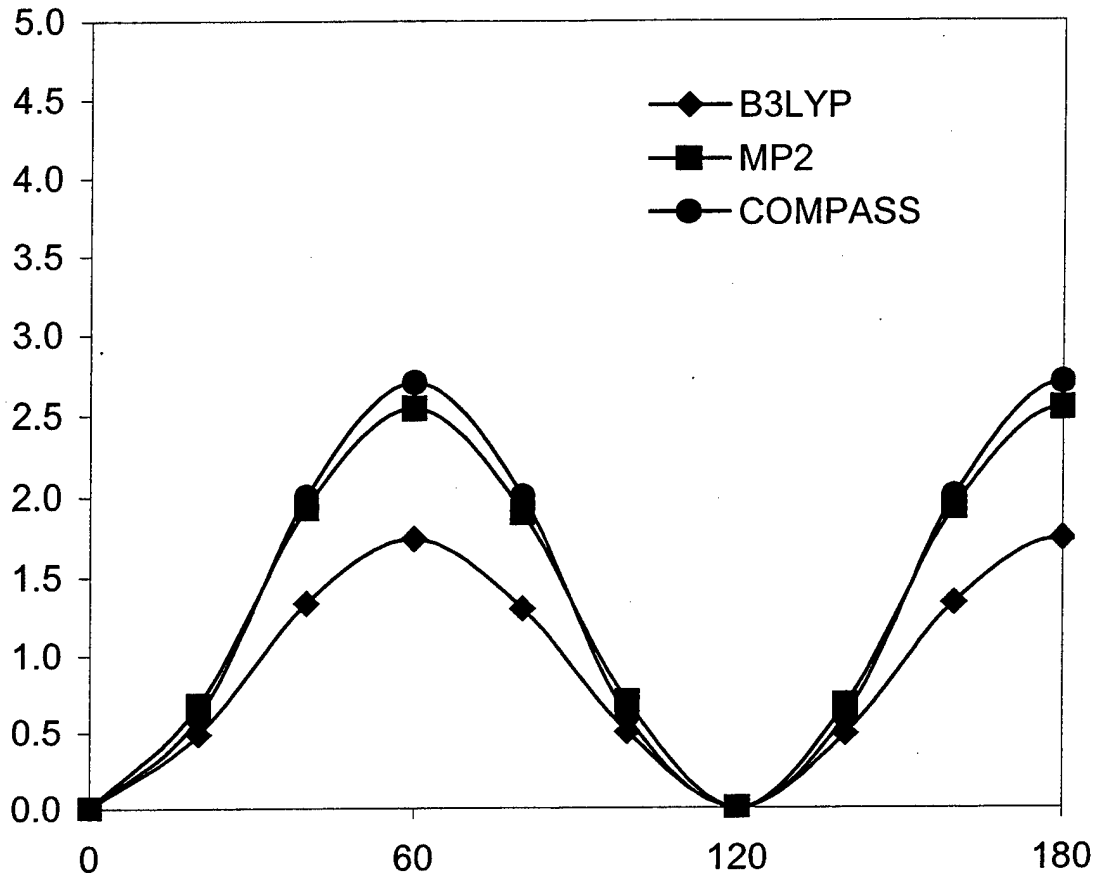

Figure 7. Energy (kcal/mol) Profile of the Rotation of the CH_3 Group About the C-O Bond of Methyl Nitrate.

4.3 Crystal Structure of Pentaerythritol Tetranitrate (PETN). Although the nonbonded parameters were optimized using liquid data, it has been shown that the COMPASS force field is capable of predicting the thermophysical properties of both liquids and crystals over an extensive range of experimental conditions. For additional validation, the present force field was used to calculate the crystal structure of PETN. The unit cell was constructed from the experimental data of Trotter [40]. The unit cell contains two independent molecules, with space-group $V_d^4 = P\bar{4}2_1c$. Figure 9 illustrates the projection of the unit cell on the *a-b* plane. For comparison purposes, we carried out both energy minimizations and NPT simulations. To rigorously test the force field parameters, the calculations were performed without any symmetry constraints (P1 space-group). In addition, all of the cell dimensions and angle parameters were fully relaxed.

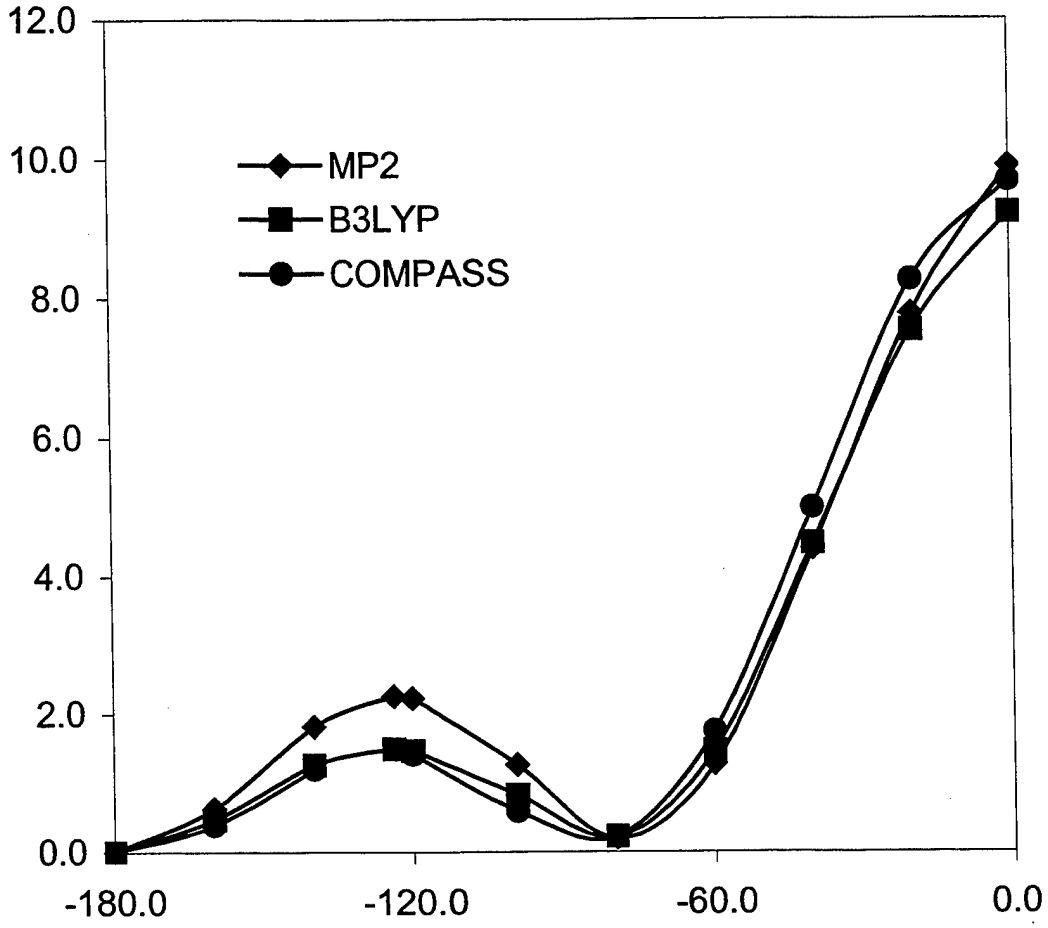

Figure 8. Energy (kcal/mol) Profile of the Rotation of the CH_3CH_2 Group About the C-O Bond of Ethyl Nitrate.

The MD simulations were done on a super cell that contained 2 × 2 × 3 unit cells. The energy minimization was performed on the unit cell. In all simulations, the Ewald summation method was used for both the electrostatic and the vdW energies.

The simulated cell parameters, densities, and lattice energies are listed in Table 11, together with the experimental data of Trotter [40]. As reported before, the energy minimization method, which corresponds to a temperature of 0° K, overestimates the density by about 5%. The computed density from a room temperature NPT simulation agrees well with the experimental data. The calculated sublimation energies are also given in this table. The experimental data are

Table 10. Liquid Nitrate Data

At Room Temperature									
	Experiment				COMPASS				
Liquids	MW	T (K)	ρ (g/cm^3)	ΔH_v (kcal/mol)	ρ (g/cm^3)	% Difference ρ (calc) - ρ (exp)	CED cal/m^3 ($x10^7$)	ΔH_v (kcal/mol)	% Difference ΔH_v (calc) - ΔH_v (exp)
Methyl Nitrate	77.04	293.2	1.2075	8.15	1.2019	-0.5	12.537	8.62	5.7
Ethyl Nitrate	91.07	293.2	1.1084	8.67	1.1063	-0.2	10.268	9.04	4.2
Isopropyl Nitrate	105.10	293.2	1.0340	9.27	1.0652	3.0	8.605	9.07	-2.1
Propyl Nitrate	105.10	293.2	1.0538	9.7	1.0517	-0.2	9.298	9.87	1.8
Butyl Nitrate	119.12	293.2	1.0228	10.42	1.0302	0.7	8.916	10.89	4.5
NG	227.09	293.2	1.5910	—	1.6232	2.0	17.467	25.02	—
DEGDN	196.12	293.2	1.3770	—	1.3785	0.1	14.331	20.97	—

At Elevated Temperature (Boiling Point)								
	Experiment				COMPASS			
Liquids	MW	T (K)	P (exp) (g/cm^3)	ΔH_v (exp) (kcal/mol)	ρ (g/cm^3)	CED cal/m^3 ($x10^v$)	ΔH_v (kcal/mol)	% Difference ΔH_v (calc) - ΔH_v (exp)
Methyl Nitrate	77.04	338.2	—	—	1.1269	10.690	7.98	—
Ethyl Nitrate	91.07	360.2	—	8.1	1.0116	8.250	8.14	0.5
Isopropyl Nitrate	105.10	373.7	—	—	0.9724	7.255	8.58	—
Propyl Nitrate	105.10	383.7	—	—	0.9331	6.935	8.57	—
Butyl Nitrate	119.12	409.7	—	—	0.8880	6.280	9.24	—
NG	227.09	450.2	—	—	1.4919	14.651	23.20	—
DEGDN	196.12	430.2	—	—	1.2300	10.860	18.17	—

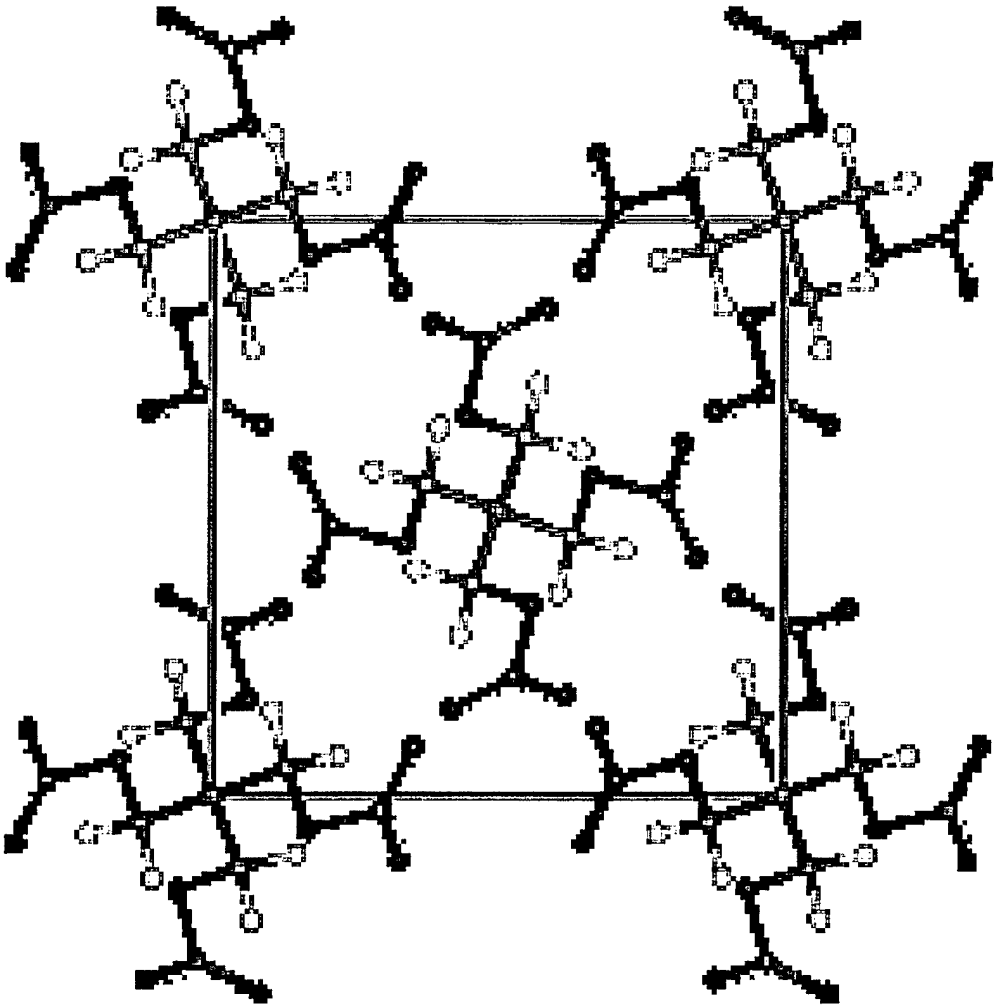

Figure 9. Projection of the Unit Cell of the PETN Crystal on the *a-b* Plane. In This Figure, Red Corresponds to Oxygen Atoms, Blue Corresponds to Nitrogen Atoms, Black Corresponds to Carbon Atoms, and White Corresponds to Hydrogen Atoms.

reported for the temperature range of 328–405 K; our NPT simulation results (293 K) agree reasonably well with the experimental value.

In addition, elastic constants of the PETN crystal were calculated using the analytical second derivative method. With the energy-minimized unit cell, the calculated values are significantly larger than the experimental data, as shown in Table 11. Considering that the

Table 11. Cell Parameters, Densities, Sublimation Energies, and Elastic Constants of PETN

	Energy Minimization (0 K)	NPT Dynamics (293 K)	Experiment[a]
Unit Cell Length (Å)			
a	9.117	9.35	9.38
b	9.117	9.35	9.38
c	6.721	6.67	6.69
Unit Cell Angle (°)			
α	90	90	90
β	90	90	90
γ	90	90	90
Density (g/cm^3)			
	1.8811	1.7997	1.7837
Sublimation Energy (kcal/mol)			
	43.58	40.49	35.95 (328–405 K)
Elastic Constants (GPa)			
	Energy Minimized Cell	Cell Dimensions Fixed	Experiment[a]
c11	21.6	13.2	17
c12	11.3	7.6	5.4
c33	16.6	11.1	n/a
c44	8.9	6.4	5
c66	6.6	6.0	n/a

[a]Experiment from reference [40].

calculation is done on a cell in which the density has been overestimated, this discrepancy is understandable. To mimic the experimental conditions, we calculated the elastic matrix with cell dimensions and angles fixed at the experimental value. Using this constraint, the results agree well with the measurement.

5. Conclusions

The COMPASS force field has been extended to include nitrate esters by combining the results of *ab initio* calculations and empirical fitting of the condensed-phase properties of methyl

and ethyl nitrate. The *ab initio* derived partial charges and geometrical parameters (bond lengths, bond angles, dihedral angles, and torsion angles) were parameterized to generate the valence parameters in the force field. The force field van der Waals terms were optimized using MD simulations of the thermophysical properties of liquid methyl and ethyl nitrate. Using the resulting force field, molecular mechanics calculations have been performed on isolated nitrates. The calculated molecular structures and vibrational frequencies agree well with experiment, high-level *ab initio*, and DFT results. In addition, room temperature simulations of the liquid properties of methyl nitrate, ethyl nitrate, propyl nitrate, butyl nitrate, isopropyl nitrate, nitroglycerin, and diethyleneglycol dinitrate have been completed. The results of these simulations agree well with the experimental data. Finally, the crystal structure, density, sublimation energy, and elastic constants of PETN have been calculated and compared to the experiment. These results suggest that this new force field is capable of predicting a range of properties of molecules containing the nitrate ester functionality in both condensed and gas phases.

INTENTIONALLY LEFT BLANK.

6. References

1. Sun, H. *Journal of Physical Chemistry B.* Vol. 102, p. 7338, 1998.

2. Sun, H., P. Ren, and J. R. Fried. *Computational and Theoretical Polymer Science.* No. 1/2, p. 229, 1998.

3 Lii, J. H., and N. L. Allinger. *Journal of the American Chemical Society.* Vol. 111, p. 8576, 1989.

4. Allinger, N. L., F. B. Li, and L. Q. Yan. *Journal of Computational Chemistry.* Vol. 11, p. 848, 1990.

5. Allinger, N. L., M. Rahman, and J. H. Lii. *Journal of the American Chemical Society.* Vol. 112, p. 8293, 1990.

6. Allinger, N. L., F. B. Li, L. Q. Yan, and J. C. Tai. *Journal of Computational Chemistry.* Vol. 11, p. 868, 1990.

7. Allinger, N. L., M. Rahman, and J. H. Lii. *Journal of the American Chemical Society.* Vol. 112, p. 8293, 1990.

8. Schmitz, L. R., and N. L. Allinger. *Journal of the American Chemical Society.* Vol. 112, p. 8307, 1990.

9. Lii, J. H., and N. L. Allinger. *Journal of Computational Chemistry.* Vol. 12, p. 186, 1991.

10. Allinger, N. L., K. S. Chen, M. Rahman, and J. Pathiaseril. *Journal of the American Chemical Society.* Vol. 113, p. 4505, 1991.

11. Allinger, N. L., M. Quinn, M. Rahman, and K. H. Chen. *Journal of Physical Organic Chemistry.* Vol. 4, p. 659, 1991.

12. Allinger, N. L. *Reviews in Computational Chemistry.* Edited by K. B. Lipkowitz and D. B. Boyd. New York: VCH Publishers, 1992.

13. Cui, W. L., F. B. Li, and N. L. Allinger. *Journal of the American Chemical Society.* Vol. 115, p. 2943, 1993.

14. Cornell, W. D., P. Cieplak, C. I. Bayly, I. R. Gould, K. M. Merz, D. M. Ferguson, D. C. Spellmeyer, T. Fox, J. W. Caldwell, and P. A Kollman. *Journal of the American Chemical Society.* Vol. 117, p. 5179, 1995.

15. Cornell, W. D., P. Cieplak, C. I. Bayly, I. R. Gould, K. M. Merz, D. M. Ferguson, D. C. Spellmeyer, T. Fox, J. W. Caldwell, and P. A. Kollman. *Journal of the American Chemical Society.* Vol. 118, p. 2309, 1996.

16. Mackerell, A. D., J. Wiorkiewiczkuczera, and M. Karplus. *Journal of the American Chemical Society.* Vol. 117, p. 11946, 1995.

17. Frisch, M. J., G. W. Trucks, H. B. Schlegel, G. E. Scuseria, M. A. Robb, J. R. Cheeseman, V. G. Zakrzewski, J. A. Montgeomery, Jr., R. E. Stratmann, J. C. Burant, S. Dapprich, J. M. Milliam, A. D. Daniels, K. N. Kudin, M. C. Strain, O. Farkas, J. Tomasi, V. Barone, M. Cossi, R. Cammi, B. Mennucci, C. Pomelli, C. Adamo, S. Clifford, J. Ochterski, G. A. Petersson, P. Y. Ayala, Q. Cui, K. Morokuma, D. K. Malick, A. D. Rabuck, K. Raghavachari, J. B. Foresman, J. Cioslowski, J. V. Ortiz, A. G. Baboul, B. B. Stefanov, G. Liu, A. Liashenko, P. Piskorz, I. Komaromi, R. Gomperts, R. L. Martin, D. J. Fox, T. Keith, M. A. Al-Laham, C. Y. Peng, A. Nanayakkara, M. Challacombe, P. M. W. Gill, B. Johnson, W. Chen, M. W. Wong, J. L. Andres, C. Gonzales, M. Head-Gordon, E. S. Replogle, and J. A. Pople. *Gaussian 94 (Revision E.2).* Pittsburgh: Gaussian, Inc., 1995.

18. Cox, A. P., and S. Waring. *Transactions of the Faraday Society.* Vol. 67, p. 3441, 1971.

19. Scroggin, D. G., J. M. Riveros, and E. B. Wilson. *Journal of Chemical Physics.* Vol. 60, p. 1376, 1974.

20. Durig, J. R., and T. G. Sheehan. *Journal of Raman Spectroscopy.* Vol. 21, p. 635, 1990.

21. Hwang, M. J., T. P. Stockfisch, and A. T. Hagler. *Journal of the American Chemical Society.* Vol. 116, p. 2515, 1994.

22. Maple, F. R., M. J. Hwang, T. P. Stockfisch, U. Dinur, M. Waldman, C. S. Ewig, and A. T. Hagler. *Journal of Computational Chemistry.* Vol. 15, p. 162, 1994.

23. Maple, J. R., M. J. Hwang, T. P. Stockfisch, A. T. Hagler. *Israeli Journal of Chemistry.* Vol. 34, p. 195, 1994.

24. Peng, Z. W., C. S. Ewig, M. J. Hwang, M. Waldman, and A. T. Hagler. *Journal of Physical Chemistry A.* Vol. 101, p. 7243, 1997.

25. Sun, H. *Journal of Computational Chemistry.* Vol. 15, p. 752, 1994.

26. Sun, H., S. J. Mumby, J. R. Maple, and A. T. Hagler. *Journal of the American Chemical Society.* Vol. 116, p. 2978, 1994.

27. Sun, H. *Macromolecules.* Vol. 28, p. 701, 1995.

28. Sun, H. *Macromolecules.* Vol. 26, p. 5924, 1994.

29. Sun, H., S. J. Mumby, J. R. Maple, and A. T. Hagler. *Journal of Physical Chemistry.* Vol. 99, p. 5873, 1995.

30. Waldman, M., and A. T. Hagler. *Journal of Computational Chemistry.* Vol. 14, p. 1077, 1993.

31. Sun, H., and D. Rigby. *Spectrochimica Acta.* Vol. A53, p. 1301, 1997.

32. Rigby, D., H. Sun, and B. E. Eichinger. *Polymer International.* Vol. 44, p. 311, 1997.

33. Frenkel, D., and B. Smit. *Understanding Molecular Simulations.* London: Academic Press, 1996.

34. Allen, M. P., and D. J. Tildesley. *Computer Simulation of Liquids.* Oxford: Clarendon Press, 1987.

35. Andersen, H. C. *Journal of Chemical Physics.* Vol. 72, p. 2384, 1980.

36. Andrea, T. A., W. C. Swope, and H. C. Andersen. *Journal of Chemical Physics.* Vol. 79, p. 4576, 1983.

37. Berendsen, H. J. C., J. P. M. Postma, W. F. van Gunsteren, A. DiNola, and J. R. Haak. *Journal of Chemical Physics.* Vol. 81, p. 3684, 1984.

38. Durig, J. R., N. E. Lindsey, and B. J. van der Veken. *Indian Journal of Pure and Applied Physics.* Vol. 26, p. 223, 1988.

39. Stull, D. R. *Industrial and Engineering Chemistry Research.* Vol. 39, p. 5147, 1947.

40. Trotter, J. *Acta.* Vol. 16, p. 698, 1963.

INTENTIONALLY LEFT BLANK.

Appendix:

New Atom Types and Parameters for Nitro Compounds and Nitrates

INTENTIONALLY LEFT BLANK.

New Atom Types and Parameters for Nitro Compounds and Nitrates

Atom types

Type	Mass	Element	Connection	Comment
n3o	14.00674	N	3	nitrogen in nitro group
o12	15.99940	O	1	oxygen in nitro group (-NO_2)
o2n	15.99940	O	2	oxygen in nitrates

Equivalences

Type	NonB	Bond	Angle	Torsion	OOP
n3o	n3o	n3o	n3o	n3o	n3o
o12	o12	o1=	o1=	o1=	o1=
o2n	o2n	o2n	o2n	o2	o2

Bond Increments

c3a	n3o	0.2390	-0.2390
c4	n3o	0.2100	-0.2100
c4	o2n	0.3170	-0.3170
c4o	n3o	0.2100	-0.2100
c4o	o2n	0.3170	-0.3170
hl	n3o	0.1880	-0.1880
n3o	o1=	0.4280	-0.4280
n3o	o2n	0.0010	-0.0010

Bond

I	J	R0	K2	K3	K4
c3a	n3o	1.4300	313.8329	-568.6087	600.9597
c4	n3o	1.4740	301.6051	-535.7028	555.0420
c4	o2n	1.4350	400.3954	-835.1951	1313.0142
c4o	n3o	1.4740	301.6051	-535.7028	555.0420
c4o	o2n	1.4350	400.3954	-835.1951	1313.0142
hl	n3o	1.0400	439.9346	-943.7307	1180.9318
n3o	o1=	1.2100	765.0664	-2070.2830	2793.3218
n3o	o2n	1.4020	300.0000	-1000.0000	2000.0000

Angle

I	J	K	Theta0	K2	K3	K4
c3a	c3a	n3o	118.8000	29.2436	-8.8495	-6.6020
hl	c4	n3o	107.0000	54.9318	-9.1333	-11.5434
hl	c4	o2n	108.7280	58.5446	-10.8088	-12.4006
c3a	n3o	o1=	117.7000	63.9404	-18.4524	-14.3129
c4	n3o	o1=	117.5000	64.5228	-18.4582	-14.4215
hl	n3o	o1=	115.7000	53.8034	-14.1991	-11.8708
o1=	n3o	o1=	128.0000	95.1035	-47.4240	-27.9164
c4	o2n	n3o	108.5000	55.7454	-10.0067	-6.2729
c4	c4	o2n	105.0000	54.5381	-8.3642	-13.0838
o2n	n3o	o1=	112.8000	85.5228	-18.4582	-14.4215

Torsion

I	J	K	L	V(1)	V(2)	V(3)
c3a	c3a	c3a	n3o	0.0000	7.2124	0.0000
hl	c3a	c3a	n3o	0.0000	2.9126	0.0000
c3a	c3a	n3o	o1=	0.0000	1.1600	0.0000
c4	c4	n3o	o1=	0.0000	0.0000	-0.3500
hl	c4	n3o	o1=	0.0000	0.0000	-0.3500
c4	c4	o2	n3o	0.0000	-0.4000	-0.2000
o1=	n3o	o2	c4	0.0000	2.0000	0.0000

Wilson out of plane

I	J	K	L	KChi	Chi0
c3a	c3a	c3a	n3o	0.9194	0.0000
c3a	n3o	o1=	o1=	36.2612	0.0000
c4	n3o	o1=	o1=	44.3062	0.0000
hl	n3o	o1=	o1=	38.5581	0.0000
o1=	n3o	o1=	o2	45.0000	0.0000

Nonbond(LJ9-6)

I	r	ε
n3o	3.7600	0.04800
o12	3.4000	0.04800
o2n	3.6500	0.20000

Bond-bond

I	J	K	K(b,b')
c3a	c3a	n3o	21.0495
c4	c4	o2n	11.4318
hl	c4	n3o	3.3770
hl	c4	o2n	23.1979
c3a	n3o	o1=	93.7948
o2n	n3o	o1=	80.0000
c4	n3o	o1=	48.1403
hl	n3o	o1=	14.8266
o1=	n3o	o1=	265.7106

Bond-angle

I	J	K	K(b,theta)	K(b',theta)
c3a	c3a	n3o	30.5211	59.8025
c4	c4	o2n	2.6868	20.4033
hl	c4	n3o	12.2491	30.5314
hl	c4	o2n	4.6189	55.3270
c3a	n3o	o1=	40.3757	92.1955
c4	n3o	o1=	27.2141	93.9927
hl	n3o	o1=	-8.6275	58.6036
o1=	n3o	o1=	95.6936	

Angle-torsion

				LEFT			RIGHT		
I	J	K	L	F(1)	F(2)	F(3)	F(1)	F(2)	F(3)
c3a	c3a	c3a	n3o	0.0000	7.7594	0.0000	0.0000	0.0000	0.0000
hl	c3a	c3a	n3o	0.0000	-8.0369	0.0000	0.0000	0.0000	0.0000
c3a	c3a	n3o	o1=	0.0000	0.0000	0.0000	0.0000	-3.4207	0.0000
hl	c4	n3o	o1=	0.0000	-0.3086	0.0000	0.0000	1.0352	0.0000
o1=	n3o	o2	c4	-3.0000	0.0000	0.0000	0.0000	0.0000	0.0000

Angle-angle-torsion

I	J	K	L	K(Ang,Ang,Tor)
c3a	c3a	c3a	n3o	-34.9681
hl	c3a	c3a	n3o	2.1508
3a	c3a	n3o	o1=	-18.0436
hl	c4	n3o	o1=	-16.2615

INTENTIONALLY LEFT BLANK.

NO. OF COPIES	ORGANIZATION
2	DEFENSE TECHNICAL INFORMATION CENTER DTIC DDA 8725 JOHN J KINGMAN RD STE 0944 FT BELVOIR VA 22060-6218
1	HQDA DAMO FDT 400 ARMY PENTAGON WASHINGTON DC 20310-0460
1	OSD OUSD(A&T)/ODDDR&E(R) R J TREW THE PENTAGON WASHINGTON DC 20301-7100
1	DPTY CG FOR RDA US ARMY MATERIEL CMD AMCRDA 5001 EISENHOWER AVE ALEXANDRIA VA 22333-0001
1	INST FOR ADVNCD TCHNLGY THE UNIV OF TEXAS AT AUSTIN PO BOX 202797 AUSTIN TX 78720-2797
1	DARPA B KASPAR 3701 N FAIRFAX DR ARLINGTON VA 22203-1714
1	US MILITARY ACADEMY MATH SCI CTR OF EXCELLENCE MADN MATH MAJ HUBER THAYER HALL WEST POINT NY 10996-1786
1	DIRECTOR US ARMY RESEARCH LAB AMSRL D D R SMITH 2800 POWDER MILL RD ADELPHI MD 20783-1197

NO. OF COPIES	ORGANIZATION
1	DIRECTOR US ARMY RESEARCH LAB AMSRL DD 2800 POWDER MILL RD ADELPHI MD 20783-1197
1	DIRECTOR US ARMY RESEARCH LAB AMSRL CI AI R (RECORDS MGMT) 2800 POWDER MILL RD ADELPHI MD 20783-1145
3	DIRECTOR US ARMY RESEARCH LAB AMSRL CI LL 2800 POWDER MILL RD ADELPHI MD 20783-1145
1	DIRECTOR US ARMY RESEARCH LAB AMSRL CI AP 2800 POWDER MILL RD ADELPHI MD 20783-1197
	ABERDEEN PROVING GROUND
4	DIR USARL AMSRL CI LP (BLDG 305)

NO. OF
COPIES ORGANIZATION

ABERDEEN PROVING GROUND

31 DIR USARL
AMSRL WM BD
W R ANDERSON
R A BEYER
A BIRK
A L BRANT
S W BUNTE
C F CHABALOWSKI
L M CHANG
T P COFFEE
J COLBURN
P J CONROY
R A FIFER
B E FORCH
B E HOMAN
S L HOWARD
P J KASTE
A J KOTLAR
C LEVERITT
K L MCNESBY
M MCQUAID
M S MILLER
T C MINOR
A W MIZIOLEK
J B MORRIS
J A NEWBERRY
M J NUSCA
R A PESCE-RODRIGUEZ
G P REEVES
B M RICE
R C SAUSA
J A VANDERHOFF
A W WILLIAMS

REPORT DOCUMENTATION PAGE

Form Approved
OMB No. 0704-0188

1. AGENCY USE ONLY *(Leave blank)*	2. REPORT DATE	3. REPORT TYPE AND DATES COVERED
	November 2000	Final, Oct 99 - Mar 00

4. TITLE AND SUBTITLE
Molecular Modeling of Energetic Materials: The Parameterization and Validation of Nitrate Esters in the COMPASS Force Field

5. FUNDING NUMBERS
622618.H80

6. AUTHOR(S)
Steven W. Bunte and Huai Sun*

7. PERFORMING ORGANIZATION NAME(S) AND ADDRESS(ES)
U.S. Army Research Laboratory
ATTN: AMSRL-WM-BD
Aberdeen Proving Ground, MD 21005-5066

8. PERFORMING ORGANIZATION REPORT NUMBER
ARL-TR-2364

9. SPONSORING/MONITORING AGENCY NAMES(S) AND ADDRESS(ES)

10.SPONSORING/MONITORING AGENCY REPORT NUMBER

11. SUPPLEMENTARY NOTES
*Molecular Simulations, Inc., 9685 Scranton Road, San Diego, CA 92121

12a. DISTRIBUTION/AVAILABILITY STATEMENT
Approved for public release; distribution is unlimited.

12b. DISTRIBUTION CODE

13. ABSTRACT *(Maximum 200 words)*

To investigate the mechanical and other condensed phase properties of energetic materials using atomistic simulation techniques, the COMPASS force field has been expanded to include high-energy nitro functional groups. This report presents the parameterization and validation of COMPASS for nitrate esters ($-ONO_2$). The functional forms of this force field are of the consistent force field type. The parameters were derived with an emphasis on the nonbonded parameters, which include a
Lennard-Jones 9-6 function for the van der Waals (vdW) term and a Coulombic term for an electrostatic interaction. To validate the force field, molecular mechanics calculations and molecular dynamics simulations have been made on a variety of molecules containing the nitrate ester functionality. Using this force field, excellent agreement has been obtained between the calculated and experimental values for molecular structures, vibrational frequencies, liquid densities, heats of vaporization, crystal structure, mechanical properties and lattice energy.

14. SUBJECT TERMS	15. NUMBER OF PAGES
molecular modeling, nitrate esters	45
	16. PRICE CODE

17. SECURITY CLASSIFICATION OF REPORT	18. SECURITY CLASSIFICATION OF THIS PAGE	19. SECURITY CLASSIFICATION OF ABSTRACT	20. LIMITATION OF ABSTRACT
UNCLASSIFIED	UNCLASSIFIED	UNCLASSIFIED	UL

INTENTIONALLY LEFT BLANK.

USER EVALUATION SHEET/CHANGE OF ADDRESS

This Laboratory undertakes a continuing effort to improve the quality of the reports it publishes. Your comments/answers to the items/questions below will aid us in our efforts.

1. ARL Report Number/Author ARL-TR-2364 (Bunte) Date of Report November 2000

2. Date Report Received _____

3. Does this report satisfy a need? (Comment on purpose, related project, or other area of interest for which the report will be used.) _____

4. Specifically, how is the report being used? (Information source, design data, procedure, source of ideas, etc.) _____

5. Has the information in this report led to any quantitative savings as far as man-hours or dollars saved, operating costs avoided, or efficiencies achieved, etc? If so, please elaborate. _____

6. General Comments. What do you think should be changed to improve future reports? (Indicate changes to organization, technical content, format, etc.) _____

CURRENT ADDRESS

_____
Organization

_____
Name E-mail Name

_____
Street or P.O. Box No.

_____
City, State, Zip Code

7. If indicating a Change of Address or Address Correction, please provide the Current or Correct address above and the Old or Incorrect address below.

OLD ADDRESS

_____
Organization

_____
Name

_____
Street or P.O. Box No.

_____
City, State, Zip Code

(Remove this sheet, fold as indicated, tape closed, and mail.)

(DO NOT STAPLE)